

# Weakly supervised segmentation with cross-modality equivariant constraints

Gaurav Patel and Jose Dolz

**Abstract**—Weakly supervised learning has emerged as an appealing alternative to alleviate the need for large labeled datasets in semantic segmentation. Most current approaches exploit class activation maps (CAMs), which can be generated from image-level annotations. Nevertheless, resulting maps have been demonstrated to be highly discriminant, failing to serve as optimal proxy pixel-level labels. We present a novel learning strategy that leverages self-supervision in a multi-modal image scenario to significantly enhance original CAMs. In particular, the proposed method is based on two observations. First, the learning of fully-supervised segmentation networks implicitly imposes equivariance by means of data augmentation, whereas this implicit constraint disappears on CAMs generated with image tags. And second, the commonalities between image modalities can be employed as an efficient self-supervisory signal, correcting the inconsistency shown by CAMs obtained across multiple modalities. To effectively train our model, we integrate a novel loss function that includes a within-modality and a cross-modality equivariant term to explicitly impose these constraints during training. In addition, we add a KL-divergence on the class prediction distributions to facilitate the information exchange between modalities, which, combined with the equivariant regularizers further improves the performance of our model. Exhaustive experiments on the popular multi-modal BRATS dataset demonstrate that our approach outperforms relevant recent literature under the same learning conditions.

**Index Terms**—Weakly supervised segmentation, multi-modal segmentation, self-training, equivariant constraints

## I. INTRODUCTION

SEMANTIC segmentation is of pivotal importance in medical image analysis, as it serves as precursor for many downstream tasks, such as diagnosis, treatment or follow-up. With the advent of deep learning, state-of-the-art in medical image segmentation is dominated by these models [1]–[3], which largely outperform more traditional methods. Nevertheless, these models require large labeled datasets, which is a cumbersome process and require user-expertise. Thus, novel learning approaches that can alleviate the need of large labeled datasets are highly desirable.

Weakly supervised segmentation (WSS) has appeared as an appealing alternative to fully-supervised learning to overcome the scarcity on annotations. In this scenario, supervision is typically given in the form of image tags [4], points [5], scribbles

Gaurav Patel is with Purdue University, West Lafayette, IN 47907, USA (e-mail: {pate1332, gpatel10}@purdue.edu).

Jose Dolz is with École de Technologie Supérieure, Montreal, QC H3C 1K3, Canada (e-mail: jose.dolz@etsmtl.ca).

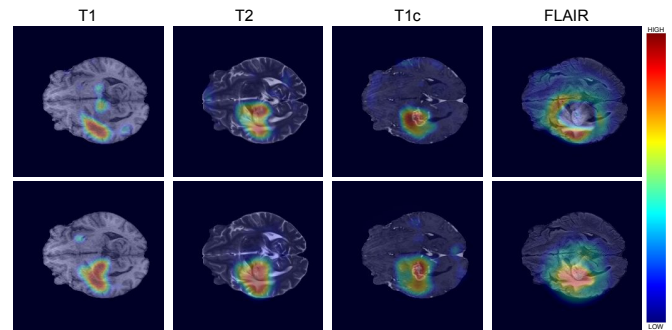


Fig. 1: Class activation maps (CAMs) obtained for different image modalities (represented as columns). The baseline CAM [13] is depicted in the *top* row, whereas CAMs obtained by the proposed model are shown in the *bottom* row.

[6], bounding boxes [7], [8] or global target information, such as object size [9]–[12]. A common strategy is to use image-level labels to derive pixel-wise class activation maps (CAMs) [13], which serve to identify object regions in the image. The resulting maps, however, are highly discriminative on the target object, while fail to correctly locate background regions, resulting in either under- or over-segmentations. To address this issue, different alternatives to improve the initial CAMs have been proposed. While combining CAMs with saliency maps is a popular choice [14], [15], other approaches resort to iterative region mining strategies [16].

Despite the wide adoption of CAMs for weakly supervised segmentation, and to the best of our knowledge, two important facts have been overlooked in the current literature. First, data augmentation is widely employed in the training of fully-supervised segmentation models. During this stage, several affine transformations are applied equally to both the input images and their corresponding pixel masks, which implicitly introduces an equivariant constraint to the model. Nevertheless, this implicit constraint is lost in the resulting CAMs, as they are obtained from the image level labels. This is evidenced in large inconsistencies on CAMs found across different affine transformations of a given image. Nevertheless, only the recent work in [17] exploited this observation to enhance the generated CAMs. And second, as shown in Figure 1, CAMs generated from the same image across different modalities are also inconsistent, despite they represent the same region.

Inspired by these limitations, we present in this paper a novel learning strategy for weakly supervised segmentation

in a multi-modal scenario. Particularly, to leverage the complementary information across image modalities we integrate three different terms in the learning objective. First, explicit intra-modality constraints enhance individual CAMs by forcing them to be similar across spatial image transformations. Second, in order to facilitate the information exchange across multiple networks, we integrate a Kullback-Leibler (KL) term on the networks outputs. Nevertheless, as we show in our experiments, this cross-modality information flow does not necessarily guarantee improvements on the object localization. To overcome this issue, we introduce a cross-modality equivariant constraint, which applies consistency regularization on the CAMs generated across modalities. This regularization provides a mechanism of self-supervision which leads to enhanced CAMs, as we show in Figure 1. Thus, the main contributions of this work can be summarized as:

- We propose a novel and effective weakly supervised segmentation strategy in the multi-modal imaging scenario.
- The proposed learning strategy leverages multi-modal images to generate enhanced CAMs under image-level supervision. In particular, we introduce intra-modality and cross-modality equivariant constraints, which guide the multi-modal learning, leading to better object localizations.
- We conduct extensive experiments on the popular BRATS dataset, demonstrating that the proposed consistency regularization terms bring a substantial gain on performance over the current state-of-the-art on weakly supervised segmentation.
- Furthermore, we also provide insights on the source of the improvement from the proposed method.

## II. RELATED WORK

### A. Weakly supervised segmentation

In contrast to fully supervised learning, deep networks trained under the weakly supervised learning paradigm make use of weak labels for training guidance. We can broadly categorize these methods as data-driven ([4], [6], [18]–[20]) and knowledge-driven approaches ([9], [21]–[24]). In the first category supervision can come in the form of image-level labels [4], [18], scribbles [6] or bounding boxes [19], [20], for example. On the other hand, the supervision in the second group is given as a prior knowledge, such as target size [9], [21], location [22] or existence of high contrast between background and foreground, i.e., saliency [23], [24]. Note that both data-driven and knowledge-driven information can be used jointly in a single approach [14], [25]. A popular strategy, however, is to resort to image-level labels to generate class activation map (CAM) [26], which are later employed as pixel-wise pseudo-masks to train segmentation networks, mimicking full supervision. As original CAMs are highly discriminative, resulting in under segmentations of the object of interest, a large body of literature has focused on enhancing these initial CAMs. A common choice to expand the initial seeds is to integrate saliency information [14], [15], [18]. For example, Kolesnikov *et al.* [18] exploited a seed-expand-constraint framework where class-independent saliency maps

[27] were used to refine initial CAMs. Other approaches rely on iterative mining strategies [16], [28], which progressively expand object regions to eventually constitute a more complete object usable for semantic segmentation. More recently, and closely related to our work, Wang *et al.* [17] proposed an equivariant attention mechanism which serves as a regularizer for the CAMs in color images.

Despite the wide use of these methods in computer vision, the literature on medical image segmentation remains scarce. DeepCut [7], which is strongly inspired by [29], resorts to the popular GrabCut [30] approach to generate image-proposals from bounding box annotations. These proposals are later used as pseudo-masks to train a segmentation network. More recently, image-level labels have also been leveraged to generate initial seeds, i.e., CAMs [31]–[33], which, similar to [7], serve as pseudo-masks in a later step. Knowledge-driven approaches prevail in the medical domain, where the prior-knowledge is typically integrated as an augmented loss function [8], [10], [11], [34]. For example, Kervadec *et al.* [10] force the segmentation output to satisfy a given region size. This term is integrated as a differentiable penalty that enforces inequality constraints directly in the learning objective.

Nevertheless, these approaches have overlooked the complementary information contained in multi-modal data which, as we will demonstrate, substantially helps to obtain more meaningful regions.

### B. Self-training

Self-training has recently attracted considerable attention as a proxy to learn robust representations. In this learning paradigm, labels can be obtained from unlabeled images via pre-text tasks. Classical pre-text tasks include predicting image orientation [35] or relative position prediction [36], solving jigsaw puzzles [37], image inpainting [38], colorization [39] and many others [40]–[43]. More recently, equivariance has been employed to impose semantic consistency, either at key-points [44], class activations [45], feature representations [46] or the network outputs [47]. Nevertheless, a main limitation of these works is that equivariance is enforced across affine transformations of the same image [17], [46], [48] or between virtually generated versions [47]. For example, Hung *et al.* [47] further apply an appearance perturbation (e.g., color jittering) to the input image before the affine transformation. The limitation of this approach is that, even though the images present appearance differences, these are not complimentary as in the case of multiple MRI modalities. Contrary to these works, we advocate that enforcing equivariant constraints across multiple image modalities results in representations that are more robust to image variations. This is particularly important in medical imaging, where each modality highlights different tissue properties.

### C. Multi-modal segmentation

Combining multiple image modalities has been extensively employed to learn more powerful representations in multi-modal fully-supervised scenarios. In this context, early and late fusion are commonly used. In particular, early fusion involves

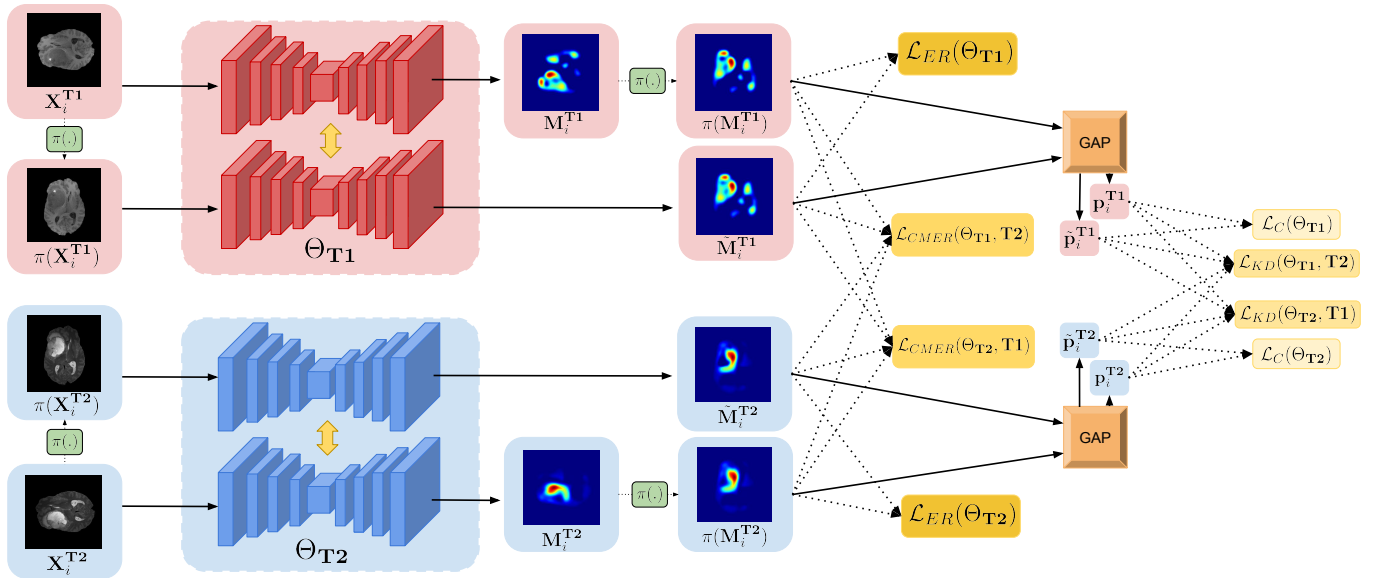


**Fig. 2:** Overview of the proposed weakly supervised learning strategy for multi-modal images under equivariant constraints. Particularly, we show the pipeline for the two-modalities setting, i.e., T1 and T2. The Each of the blocks processing single modalities are depicted in colors (red and blue). Then, we employ different shades of yellow to represent the multiple loss terms employed for training. Our model enhances the class activation maps in multi-modal imaging by coupling an intra-modality and a cross-modality equivariant constraint (Section III-B). Furthermore, the KL terms ( $\mathcal{L}(\Theta_{m_1}, m_2)$  and  $\mathcal{L}(\Theta_{m_2}, m_1)$ ) facilitate the information exchange between modalities.

concatenating the multiple modalities in the input of the network, each representing an individual channel [49], [50]. On the other hand, late fusion promotes processing modalities individually, whose features are fused in a later stage [51], [52], typically at the last convolutional layers. In addition, there exist recent works that present more sophisticated multi-modal fusion strategies. These models include leveraging dense connectivity [53] or multi-scale fusion strategies [54], among others. However, despite the increasing interest seen in multi-modal segmentation, the literature has mostly focused on fully-supervised tasks. Thus, our work contrasts to prior literature, as we aim at leveraging multi-modal information under the weakly supervised learning paradigm.

### III. METHODOLOGY

#### A. Formulation

Let us denote a set of  $N$  training images as  $\mathcal{D} = \{(\{\mathbf{X}_i^{m_k}\}_{k=1}^K, \mathbf{y}_i)\}_{i=1}^N$  where  $\mathbf{X}_i^{m_k} \in \mathbb{R}^{\Omega_i^{m_k}}$  is an image belonging to modality  $m_k$ ,  $K$  denotes the total number of modalities,  $\Omega_i^{m_k}$  denotes the spatial image dimension and  $\mathbf{y}_i \in \{0, 1\}^C$  its corresponding one-hot encoded class label, with  $C$  indicating the number of distinct classes. Furthermore, we denote  $\mathcal{P} = \{\{\mathbf{p}_i^{m_k}\}_{k=1}^K\}_{i=1}^N$  as the set of corresponding vectors of softmax probabilities, obtained from the final classification layer, where  $\mathbf{p}_i^{m_k} = f_{\Theta_{m_k}}(\mathbf{X}_i^{m_k}) \in [0, 1]^C$ , being  $f_{\Theta_{m_k}}(\cdot)$  a convolutional neural network parameterized by  $\Theta_{m_k}$ . Additionally, following the literature in weakly supervised segmentation, we can obtain the corresponding

image class activation maps (CAMs<sup>1</sup>) from samples in  $\mathcal{D}$ , resulting in the set  $\mathcal{M} = \{\{\mathbf{M}_i^{m_k}\}_{k=1}^K\}_{i=1}^N$ . In this set,  $\mathbf{M}_i^{m_k} \in [0, 1]^{\Omega_i^{m_k} \times C-1}$ <sup>2</sup> represents the max-normalized CAM of the  $i^{\text{th}}$  sample and modality  $m_k$ .

#### B. Self-supervision with Transformation Equivariance

Many WSS methods jointly leverage classification and segmentation models by training a classification network first and then keeping part of the network as features extractor to tackle the segmentation task. Take for example a segmentation neural network  $f_{\Theta_s}(\cdot)$ , which produces a pixel-mask segmentation  $\hat{\mathbf{Y}} = f_{\Theta_s}(\mathbf{X})$  for a given image  $\mathbf{X}$ . According to the literature in WSS, this model can be transformed into a classification network by simply adding a pooling layer,  $\hat{\mathbf{y}} = \text{Pool}(f_{\Theta_s}(\mathbf{X}))$ , as they are built on the assumption that learned parameters are equivalent. Nevertheless, despite the commonalities between these networks, there exist underlying differences that can be exploited in the context of semantic segmentation. Particularly, while the former is transformation invariant –random image transformations should lead to the same prediction–, the latter is transformation equivariant. This means that for a random spatial image transformation  $\pi(\cdot)$ , the pixel-wise prediction should be affected identically,  $f_{\Theta_s}(\pi(\mathbf{X})) = \pi(f_{\Theta_s}(\mathbf{X}))$ . This motivates the integration of equivariance properties in the learning objective, which can result in strong regularizers that allow an explicit mechanism to include equivariant constraints.

<sup>1</sup>Note that in our implementation we use the single-step alternative to obtaining the CAM as in [55], which avoids the additional weight multiplication of the fully-connect layers with the feature maps as in the original CAMs [13].

<sup>2</sup>The class activation map corresponding to the background class is not included, therefore this results in a vector of dimension  $C - 1$ .

We first generate an augmented training set where each image in  $\mathcal{D}$  follows a series of spatial transformations  $\pi(\cdot)$ , resulting in  $\mathcal{D}_\pi = \{\{\pi(\mathbf{X}_i^{m_k})\}_{k=1}^K, \mathbf{y}_i\}_{i=1}^N$ . Note that each image follows the same transformation across the  $K$  modalities. Then, we generate their corresponding CAMs, which are denoted as  $\mathcal{M}_\pi = \{\{\tilde{\mathbf{M}}_i^{m_k}\}_{k=1}^K\}_{i=1}^N$ , and obtain the softmax vector probabilities on the transformed images,  $\mathcal{P}_\pi = \{\{\tilde{\mathbf{p}}_i^{m_1}\}_{k=1}^K\}_{i=1}^N$ . For simplicity and the ease of explanation we formulate our method in a bi-modal setup, with image modalities  $m_1$  and  $m_2$  operated on networks with weights  $\Theta_{m_1}$  and  $\Theta_{m_2}$ , respectively, and later generalize to  $K$  modalities.

a) **Within modalities equivariance:** Equivariant regularizers on single modalities have been recently explored in weakly-supervised [17] and self-supervised [46] learning. This explicit constraint can be formally defined as:

$$\mathcal{R}_E = \|\pi(f(\mathbf{X})) - f(\pi(\mathbf{X}))\|_2^2 \quad (1)$$

where  $f(\cdot)$  could be the same network [46] or an expanded version consisting in a shared-weight Siamese structure with two branches [17]. Following these works, we define the first of our objective terms, a transformation equivariance regularization loss, which enforces transformation consistency within the same modality:

$$\mathcal{L}_{ER}(\Theta_{m_1}) = \|\pi(\mathbf{M}_i^{m_1}) - \tilde{\mathbf{M}}_i^{m_1}\|_2^2 \quad (2)$$

b) **Information exchange across multiple networks:** In addition to single-modality equivariance, we aim at facilitating information flow across networks, each corresponding to individual modalities  $m_1$  and  $m_2$ . To achieve this, we first enforce the softmax likelihood from the first network,  $\mathbf{p}_i^{m_1}$ , to match the posterior probability from the second network,  $\mathbf{p}_i^{m_2}$ , for both original and transformed images. This is similar to [56], [57], where cross-modal distillation was employed as a supervisory signal in the context of object region detection and classification. The resulting objective can be formulated as a Kullback-Leibler (KL) divergence term:

$$\mathcal{L}_{KD}(\Theta_{m_1}, m_2) = \frac{1}{2}(\mathcal{D}_{KL}(\mathbf{p}_i^{m_2} \|\mathbf{p}_i^{m_1}) + \mathcal{D}_{KL}(\tilde{\mathbf{p}}_i^{m_2} \|\tilde{\mathbf{p}}_i^{m_1})) \quad (3)$$

where  $\mathcal{D}_{KL}(\mathbf{p} \|\mathbf{q}) = \mathbf{p}^\top \log(\frac{\mathbf{p}}{\mathbf{q}})$ . We resort to  $\mathcal{L}_{KD}(\cdot, m_k)$  to emphasize that the knowledge is distilled from the  $k$ -th modality. Note that our KL divergence loss is asymmetric and thus different for each network, which explains the need of using two asymmetric terms. Instead, we could have used a symmetric Jensen-Shannon Divergence loss, but [57] observed that empirically employing either a symmetric or an asymmetric KL loss does not make any difference.

Nevertheless, information exchange on the predicted likelihood distribution does not guarantee improvement on object localization, as we will show in the experimental section. Thus, inspired from [58] we seek to mine complementary information present in CAMs derived from multiple modalities. To achieve this, we impose equivariance constraints on multi-modal CAMs, which we refer to as the Cross-Modal Equivariance Regularization (CMER) loss, defined as:

$$\begin{aligned} \mathcal{L}_{CMER}(\Theta_{m_1}, m_2) = & \frac{1}{2} \left( \left\| \pi\left(\frac{\mathbf{M}_i^{m_2}}{\|\mathbf{M}_i^{m_2}\|_2}\right) - \frac{\tilde{\mathbf{M}}_i^{m_1}}{\|\tilde{\mathbf{M}}_i^{m_1}\|_2} \right\|_2^2 \right. \\ & \left. + \left\| \frac{\tilde{\mathbf{M}}_i^{m_2}}{\|\tilde{\mathbf{M}}_i^{m_2}\|_2} - \pi\left(\frac{\mathbf{M}_i^{m_1}}{\|\mathbf{M}_i^{m_1}\|_2}\right) \right\|_2^2 \right) \quad (4) \end{aligned}$$

### C. Classification loss

In the context of this work, we only have access to image-level labels as supervisory signals. To leverage this information, we integrate a global average pooling layer at the end of the model (Fig. 2). The role of this layer is to aggregate the CAMs derived from the original and transformed images at each branch into the prediction vectors  $\mathbf{p}^{m_k}$  and  $\tilde{\mathbf{p}}^{m_k}$ , respectively, for image classification. To train the network we resort to the standard cross-entropy loss  $\mathcal{L}_{CE}(\mathbf{p}, \mathbf{y}) = -\mathbf{y}^\top \log(\mathbf{p})$ , where  $\mathbf{p}$  and  $\mathbf{y}$  are the row vectors of length  $C$  of the predicted softmax probabilities and the one-hot encoded ground-truth, respectively. As we employ a siamese structure to impose the self-equivariance, we extend the image-level supervision to both the branches. Thus, for the network processing the  $k$ -th modality, the classification loss becomes:

$$\mathcal{L}_C(\Theta_{m_k}) = \frac{1}{2}(\mathcal{L}_{CE}(\mathbf{p}_i^{m_k}, \mathbf{y}_i) + \mathcal{L}_{CE}(\tilde{\mathbf{p}}_i^{m_k}, \mathbf{y}_i)). \quad (5)$$

### D. Global objective

Finally, the overall loss function for our model can be defined as  $\mathcal{L} = \mathcal{L}(\Theta_{m_1}) + \mathcal{L}(\Theta_{m_2})$ , where each term represents the loss for each network. Particularly, for the model parameterized by  $\Theta_{m_1}$ , this loss can be defined as:

$$\begin{aligned} \mathcal{L}(\Theta_{m_1}) = & \mathcal{L}_C(\Theta_{m_1}) + \lambda_{KD} \mathcal{L}_{KD}(\Theta_{m_1}, m_2) \\ & + \lambda_E(t)(\mathcal{L}_{ER}(\Theta_{m_1}) + \mathcal{L}_{CMER}(\Theta_{m_1}, m_2)) \quad (6) \end{aligned}$$

where  $\lambda_{KD}$  and  $\lambda_E(t)$  balance the importance of each term in the learning objective. Similarly, for the network parameterized with  $\Theta_{m_2}$ , the overall loss function is:

$$\begin{aligned} \mathcal{L}(\Theta_{m_2}) = & \mathcal{L}_C(\Theta_{m_2}) + \lambda_{KD} \mathcal{L}_{KD}(\Theta_{m_2}, m_1) \\ & + \lambda_E(t)(\mathcal{L}_{ER}(\Theta_{m_2}) + \mathcal{L}_{CMER}(\Theta_{m_2}, m_1)) \quad (7) \end{aligned}$$

### E. Generalization to $K$ -modalities

We now generalize our learning objective to  $K$  modalities, which involves  $K$  networks learning simultaneously. For a particular network  $\Theta_{m_k}$  processing the modality  $m_k$ , the loss function can be defined as:

$$\begin{aligned} \mathcal{L}(\Theta_{m_k}) = & \mathcal{L}_C(\Theta_{m_k}) \\ & + \lambda_{KD} \left( \frac{1}{K-1} \sum_{l=1, l \neq k}^{l=K} \mathcal{L}_{KD}(\Theta_{m_k}, m_l) \right) \\ & + \lambda_E(t)(\mathcal{L}_{ER}(\Theta_{m_k}) + \frac{1}{K-1} \sum_{l=1, l \neq k}^{l=K} \mathcal{L}_{CMER}(\Theta_{m_k}, m_l)) \quad (8) \end{aligned}$$

Our learning strategy is detailed in Algo. 1.



---

**Algorithm 1** Training algorithm
 

---

**Input:** Training dataset  $\mathcal{D}$

- 1:  $K$  = Number of image modalities
- 2:  $\Pi$  = Set of transformations
- 3:  $T$  = Total number of Epochs
- 4: **for**  $k$  in  $[1, K]$  **do**
- 5:     Initialize  $\Theta_{m_k}$
- 6: **end for**
- 7: **for**  $t$  in  $[1, T]$  **do**
- 8:     **for** every minibatch  $B$  in  $\mathcal{D}$  **do**
- 9:          $\pi \leftarrow \pi \sim \Pi$
- 10:          $\mathcal{M} \leftarrow \{\{\mathbf{M}_i^{m_k}\}_{k=1}^K\}_{i \in B}$
- 11:          $\mathcal{P} \leftarrow \{\{\tilde{\mathbf{P}}_i^{m_k}\}_{k=1}^K\}_{i \in B}$
- 12:          $\mathcal{D}_\pi \leftarrow \{\{\pi(\mathbf{X}_i^{m_k})\}_{k=1}^K, \mathbf{y}_i\}_{i \in B}$
- 13:          $\mathcal{M}_\pi \leftarrow \{\{\mathbf{M}_i^{m_k}\}_{k=1}^K\}_{i \in B}$
- 14:          $\mathcal{P}_\pi \leftarrow \{\{\tilde{\mathbf{P}}_i^{m_k}\}_{k=1}^K\}_{i \in B}$
- 15:         **for**  $k$  in  $[1, K]$  **do**
- 16:             Compute  $\mathcal{L}_C(\Theta_{m_k}), \mathcal{L}_{ER}(\Theta_{m_k}),$
- 17:              $\mathcal{L}_{KD}(\Theta_{m_k}, m_{l \neq k}), \mathcal{L}_{CMER}(\Theta_{m_k}, m_{l \neq k}).$
- 18:             Compute  $\mathcal{L}(\Theta_{m_k})$
- 19:              $loss \leftarrow \frac{1}{|B|} \sum_{i \in B} \mathcal{L}(\Theta_{m_k})$
- 20:             Compute gradients of  $loss$  w.r.t  $\Theta_{m_k}$
- 21:             Update  $\Theta_{m_k}$  using the optimizer
- 22:         **end for**
- 23:     **end for**
- 24: **end for**

---

## IV. EXPERIMENTAL SETTING

### A. Dataset

We benchmark the proposed method in the context of multi-modal brain tumor segmentation in MR images. Particularly, we use the popular BraTS 2019 dataset [59]–[61]. This dataset contains 335 multi-modal scans with their corresponding expert segmentation masks. More concretely, the scans are composed of four modalities, which include T1, T1c, T2 and FLAIR. The images were re-sampled to an isotropic 1.0 mm voxel spacing, skull-stripped and co-registered by the challenge organizers. In the context of this work, we consider a binary segmentation class, i.e., healthy vs non-healthy targets. Thus, we merge the different tumour classes into a common non-healthy class. The reason behind this is based on the poor performance of CAMs, and its versions, to obtain usable initial proxy labels if the problem is tackled as a multi-class task. The dataset is finally divided into training, validation and testing set, each containing 271, 32 and 32 scans, respectively and equally stratified with respect to high-grade gliomas (HGG) and low-grade gliomas (LGG) scans in each data split.

### B. Evaluation metrics

To assess the performance of the proposed approach, we employ the common Dice Similarity coefficient (DSC) and the average symmetric surface distance (ASSD).

### C. Implementation details

All models were implemented in PyTorch [62] and use U-Net [63] as backbone architecture. To train the models, we

use AdamW [64] optimizer with a learning rate of 0.00005, a weight decay of 0.1 and a mini-batch size equal to 16. The regularization weight  $\lambda_{KD}$  was empirically set to 0.5 and  $\lambda_E(t) = \begin{cases} e^{-(t-\mathcal{T})^2} & 0 \leq t < \mathcal{T} \\ 1 & \mathcal{T} \leq t \end{cases}$  as a function of epochs  $t$  with  $\mathcal{T} = 15$ . We empirically observed that assigning large weights to the equivariance constraint terms at the beginning of the training hampered the quality of the class-activation maps. Thus, we employed a variable weighting coefficient that allows classification losses guiding the training to identify the initial CAMs, while equivariance losses gradually become important to revise the object regions across modalities. The affine image transformations include flipping, rotation, scaling, and translation. More concretely, the rotation transformation involves each image being randomly rotated with an angle equal to  $k * 90^\circ$ , where  $k \in \{0, 1, 2, 3\}$ . During scaling, the scaling ratio is selected randomly in the range  $[0.8, 1.2]$ . And last, the shifting in the translation transformation is selected randomly in the range  $-0.3 * (h, w) < (dh, dw) < 0.3 * (h, w)$ , where  $h$  and  $w$  denote the height and width dimension of the given image. To demonstrate that the proposed learning strategy is robust against the CAM approach selected, we report the results on both CAMs [13] and GradCAMs++ [65]. To obtain the final segmentation masks, we binarize all the CAMs with a threshold fixed to 0.5.

In our experiments we demonstrate the effectiveness of our approach by combining 2 and 4 modalities. In the two-modality scenario, we have created image pairs according to their *a priori* dissimilarities. More concretely, T1 and T1c are the same modality with the only difference that T1c contains a contrast agent to improve the contrast of the boundaries in regions affected by hemorrhage. On the other hand, FLAIR sequence is similar to T2, except that TE and TR times are much longer. Thus, we consider that T1 and T1c belong to one group, whereas T2 and FLAIR are included in another group. To create the image-pairs, we just combine one modality from the first group with one modality from the second group.

Experiments were run in a server with 4 Nvidia P100 GPU cards. The code and trained models are made publicly available at: <https://github.com/gaurav104/WSS-CMER>

### D. Baselines for comparison

We benchmark the proposed approach to relevant prior literature. As our approach resorts to CAM and GradCAM++ to generate the final pixel-wise segmentations, we employ them as lower bound baselines. Then, we also include SEAM [17] in our experiments. The reason behind this choice is two-fold. First, SEAM also incorporates equivariance regularizers to boost the initial CAMs. In this case, while in the original work authors report results on scale equivariance, we also evaluate their performance when including several image transformations. And second, as reported in their experiments, this method represents the current state-of-the-art in weakly supervised segmentation. Last, we also include the results from a fully-supervised model trained with a combination of the

**TABLE I:** Quantitative results compared to prior literature. Individual performance represented in the first 2 columns, whereas combined results of individual maps are depicted in the last column. Best results are highlighted in bold.

		T1		T2		T1-T2	
Method		DSC	ASSD	DSC	ASSD	DSC	ASSD
CAM	Baseline	38.66±16.27	12.25±7.08	46.80±15.90	10.83±9.05	49.81±14.78	11.04±5.73
	SEAM [17] (scale)	41.20±14.74	11.86±6.00	50.96±15.19	9.58±5.19	52.74±13.50	11.16±5.23
	SEAM [17] (all)	39.05±14.32	10.74±5.06	50.11±14.34	7.58±4.02	54.23±12.20	10.09±4.91
	Proposed	<b>47.11±14.40</b>	<b>10.43±5.55</b>	<b>58.98±12.87</b>	<b>7.44±4.35</b>	<b>59.72±11.77</b>	<b>9.91±5.09</b>
GradCAM++	Baseline	39.16±16.11	12.19±6.95	45.79±15.59	10.92±9.06	50.11±14.95	11.14±5.72
	SEAM [17] (scale)	41.94±14.46	11.86±5.85	51.34±15.23	9.66±5.25	52.70±13.61	11.32±5.21
	SEAM [17] (all)	39.08±15.27	12.20±5.45	50.56±14.14	7.60±4.06	54.43±12.13	10.20±4.96
	Proposed	<b>47.05±14.42</b>	<b>10.57±5.57</b>	<b>58.93±12.80</b>	<b>7.47±4.36</b>	<b>59.46±11.90</b>	<b>10.04±5.10</b>
		T1c		FLAIR		T1c-FLAIR	
		DSC	ASSD	DSC	ASSD	DSC	ASSD
CAM	Baseline	36.27±18.33	14.36±8.48	41.58±14.66	7.87±4.33	45.40±14.78	11.06±5.34
	SEAM [17] (scale)	40.91±17.20	12.16±4.77	41.32±15.11	<b>7.23±3.84</b>	48.01±12.81	9.62±4.45
	SEAM [17] (all)	43.38±16.79	12.40±6.52	43.04±14.40	7.77±4.67	51.31±12.44	9.61±5.01
	Proposed	<b>47.95±15.43</b>	<b>11.50±6.54</b>	<b>53.05±16.52</b>	8.34±4.44	<b>57.59±15.00</b>	<b>11.43±5.09</b>
GradCAM++	Baseline	37.23±18.60	14.35±8.45	43.36±14.42	7.89±4.39	46.32±14.77	11.21±5.38
	SEAM [17] (scale)	41.54±17.44	12.18±5.08	42.56±14.84	<b>7.23±3.84</b>	47.96±13.52	9.67±4.48
	SEAM [17] (all)	43.45±16.86	12.45±6.49	43.82±14.44	7.82±4.63	51.58±12.43	9.72±5.03
	Proposed	<b>47.88±15.41</b>	<b>11.57±6.53</b>	<b>53.02±16.46</b>	8.37±4.46	<b>57.55±15.00</b>	<b>9.44±5.09</b>
		T1		FLAIR		T1-FLAIR	
		DSC	ASSD	DSC	ASSD	DSC	ASSD
CAM	Baseline	38.66±16.27	12.25±7.08	41.58±14.66	7.87±4.33	48.42±13.53	11.04±5.73
	SEAM [17] (scale)	41.20±14.74	11.86±6.00	41.32±15.11	<b>7.23±3.84</b>	48.68±13.06	9.60±4.98
	SEAM [17] (all)	39.05±14.32	<b>10.74±5.06</b>	43.04±14.40	7.77±4.67	49.82±13.00	9.15±4.70
	Proposed	<b>47.23±13.19</b>	11.12±4.92	<b>56.20±18.76</b>	7.50±4.20	<b>58.87±15.04</b>	<b>9.01±4.66</b>
GradCAM++	Baseline	39.16±16.11	12.19±6.95	43.36±14.42	7.89±4.39	49.23±13.54	11.13±5.72
	SEAM [17] (scale)	41.94±14.46	11.86±5.85	42.56±14.84	<b>7.23±3.84</b>	49.13±13.09	9.78±4.99
	SEAM [17] (all)	39.08±15.27	12.20±5.45	43.82±14.44	7.82±4.63	50.44±12.95	9.38±4.85
	Proposed	<b>47.30±12.70</b>	<b>11.21±4.97</b>	<b>56.34±18.50</b>	7.59±4.30	<b>58.53±15.09</b>	<b>9.13±4.66</b>
		T1c		T2		T1c-T2	
		DSC	ASSD	DSC	ASSD	DSC	ASSD
CAM	Baseline	36.27±18.33	14.36±8.48	46.80±15.90	10.83±9.05	47.44±15.27	12.56±5.90
	SEAM [17] (scale)	40.91±17.20	12.16±4.77	50.96±15.19	9.58±5.19	51.53±12.82	10.82±4.69
	SEAM [17] (all)	43.38±16.79	12.40±6.52	50.11±14.34	<b>7.58±4.02</b>	56.01±11.96	10.53±5.01
	Proposed	<b>47.47±15.05</b>	<b>11.85±5.66</b>	<b>57.90±13.85</b>	8.39±5.40	<b>59.16±11.33</b>	<b>10.35±5.16</b>
GradCAM++	Baseline	37.23±18.60	14.35±8.45	45.79±15.59	10.92±9.06	47.82±15.59	12.67±5.92
	SEAM [17] (scale)	41.54±17.44	12.18±5.08	51.34±15.23	9.66±5.25	51.73±12.94	10.85±4.72
	SEAM [17] (all)	43.45±16.86	12.45±6.49	50.56±14.14	<b>7.60±4.06</b>	56.14±11.93	10.56±5.02
	Proposed	<b>47.59±15.02</b>	<b>11.92±5.62</b>	<b>57.97±13.59</b>	8.57±5.58	<b>58.93±13.41</b>	<b>10.44±5.16</b>

dice and the cross-entropy loss as the objective function, which represents the upper bound.

## V. RESULTS

### A. Quantitative results

1) *Comparison to the literature:* The results of this experiment are reported in Table I, where the first two columns show the individual results per modality and the final column contains the results when both modalities are combined. CAMs fusion is achieved by getting the maximum pixel-wise value across modalities, i.e.,  $\max(\mathbf{M}^1, \mathbf{M}^2)$ . If we look at individual-modality performances, the first thing that we can observe is that the original SEAM model, which only employs the scale transformation as equivariance regularizer, consistently improves the baselines across all modalities. Interestingly, the fact of including additional image transformations (i.e., SEAM-all) does not necessarily improve the performance, contrary to the common belief followed in standard data-augmentation strategies. Indeed, this finding aligns with the observations in [17], where authors found that simply aggregating different affine transformations does not always bring segmentation improvements. In our experiments, we demonstrate that certain modalities (i.e., T1c and FLAIR) benefit from multiple image affine transformations, whereas others (i.e., T1 and T2) see their performance degrade. Regarding the proposed method, we observe a significant improvement over the baselines, which is consistent across modalities and CAM versions. In particular, compared to the original SEAM approach [17], the proposed model brings between 6% (in T1, T1c) to 12% (in FLAIR) improvement in terms of DSC. Differences in the ASSD metric are smaller, with values ranging from 0.3 to 1 voxels, as average, for all

the modalities except FLAIR, where SEAM slightly outperforms the proposed model. Note that our method employs the same affine transformations as SEAM-all and therefore, performance differences are further magnified with respect to this model. Last, we can observe that this trend holds when fusing both modalities (*last column*). In particular, our model outperforms the second best model between nearly 3% (T1-T2) to more than 8% (T1-FLAIR). We also report the values obtained on the four modality scenario (Table II). Similar to the two-modalities setting, our model substantially improves the performance over the other models. Including multi-modal information flow during training results in performance gains between 7% and 16% in terms of DSC, such as in T1, T2 and FLAIR. If individual modality results are further combined, improvement over the baseline is around 7% compared to the original CAMs and GradCAM++. Last, our model outperforms the two settings based in [17] by 5% and nearly 2.5%. These results suggest that by facilitating information flow between modalities by means of inter-modality equivariance constraints on original CAMs significantly improves the segmentation performance.

Last, we report the results of the upper bound in Table II across individual modalities. These values show that despite our method obtains closer results to standard fully supervised learning, there are still opportunities to progress in this task.

2) *On the impact of the different objective terms:* We now assess the effect of the learning objectives integrated in our model. To this end, we report the results of four image-pairs, as well as a model containing the four modalities (Table III). These results show that including the within-modality equivariance constraint (Eq. 2) typically results in an improvement that ranges across settings. For instance, in

**TABLE II:** Quantitative results compared to prior literature. Individual performance represented in the first 4 columns, whereas combined results of individual maps are depicted in the last column. Best results are highlighted in bold.

Method	T1		T2		T1c		FLAIR		Fused		
	DSC	ASSD	DSC	ASSD	DSC	ASSD	DSC	ASSD	DSC	ASSD	
CAM	Baseline	38.66±16.27	12.25±7.08	46.80±15.90	10.83±9.05	36.27±18.33	14.36±8.48	41.58±14.66	7.87±4.33	49.64±14.05	11.28±5.46
	SEAM [17] (scale)	41.20±14.74	11.86±6.00	50.96±15.19	9.58±5.19	40.91±17.20	12.16±4.77	41.32±15.11	<b>7.23±3.84</b>	51.72±13.39	11.13±4.89
	SEAM [17] (all)	39.05±14.32	10.74±5.06	50.11±14.34	<b>7.58±4.02</b>	43.38±16.79	12.40±6.52	43.04±14.40	7.77±4.67	54.53±11.14	11.00±5.00
	Proposed	<b>47.56±14.81</b>	<b>10.31±5.01</b>	<b>57.07±14.23</b>	8.39±5.09	<b>44.74±15.99</b>	<b>11.62±6.12</b>	<b>58.64±16.42</b>	7.29±4.38	<b>56.81±13.84</b>	<b>10.80±5.01</b>
GradCAM++	Baseline	39.16±16.11	12.19±6.95	45.79±15.59	10.92±9.06	37.23±18.60	14.35±8.45	43.36±14.42	7.89±4.39	49.98±14.22	11.41±5.47
	SEAM [17] (scale)	41.94±14.46	11.86±5.85	51.34±15.23	9.66±5.25	41.54±17.44	12.18±5.08	42.56±14.84	<b>7.23±3.84</b>	51.78±13.51	11.24±4.92
	SEAM [17] (all)	39.08±15.27	12.20±5.45	50.56±14.14	<b>7.60±4.06</b>	43.45±16.86	12.45±6.49	43.82±14.44	7.82±4.63	54.64±11.17	11.07±5.02
	Proposed	<b>47.48±14.35</b>	<b>10.39±5.00</b>	<b>57.13±14.17</b>	8.42±5.12	<b>44.73±15.99</b>	<b>11.62±6.18</b>	<b>59.73±16.41</b>	7.26±4.49	<b>57.05±14.06</b>	<b>10.83±5.01</b>
Upper Bound	Full Supervision	71.40±17.15	6.37±3.71	79.60±14.88	3.04±1.87	66.54±24.42	5.27±4.26	81.80±17.10	2.30±1.50	-	-

**TABLE III:** Ablation study on the losses:  $\mathcal{L}_{KD}$  (Eq. 3),  $\mathcal{L}_{ER}$  (Eq. 2) and  $\mathcal{L}_{CMER}$  (Eq. 4). Best results in bold.

Losses	T1-T2		T1c- FLAIR		T1- FLAIR		T1c-T2		All				
	$\mathcal{L}_{KD}$	$\mathcal{L}_{ER}$	$\mathcal{L}_{CMER}$	DSC	ASSD	DSC	ASSD	DSC	ASSD	DSC	ASSD		
CAM	✓	-	-	55.91±13.93	10.46±4.68	51.39±13.46	11.92±4.85	50.08±13.51	10.87±4.72	51.39±13.46	11.92±4.85	46.44±13.98	12.07±4.80
	✓	✓	-	55.13±13.21	12.18±5.61	55.46±13.37	10.81±5.28	52.94±14.17	11.44±5.28	55.46±13.37	10.81±5.28	54.37±16.20	12.98±5.63
	-	✓	✓	<b>60.39±11.60</b>	<b>9.19±4.76</b>	57.07±11.92	11.23±5.19	57.24±14.57	9.04±4.59	57.07±11.92	11.23±5.19	55.62±14.26	11.10±4.89
	✓	✓	✓	59.72±11.77	9.91±5.09	<b>57.59±15.00</b>	<b>9.43±5.09</b>	<b>58.87±15.04</b>	<b>9.01±4.66</b>	<b>59.16±13.33</b>	<b>10.35±5.16</b>	<b>56.81±13.84</b>	<b>10.80±5.01</b>
GradCAM++	✓	-	-	55.88±13.87	10.58±4.70	51.15±13.53	12.12±4.85	50.28±13.76	11.13±4.83	51.15±13.53	12.12±4.85	46.15±14.04	12.45±4.81
	✓	✓	-	54.15±13.60	12.67±5.79	55.22±13.48	10.84±5.29	53.03±14.25	11.61±5.35	55.22±13.48	10.84±5.29	54.29±16.21	13.09±5.63
	-	✓	✓	<b>60.26±11.62</b>	<b>9.28±4.81</b>	56.80±12.01	11.38±5.18	56.99±14.62	9.30±4.76	56.80±12.01	11.38±5.18	55.43±14.28	11.2±4.89
	✓	✓	✓	59.46±11.90	10.04±5.10	<b>57.55±15.00</b>	<b>9.44±5.09</b>	<b>58.53±15.09</b>	<b>9.13±4.66</b>	<b>58.93±13.41</b>	<b>10.44±5.16</b>	<b>57.05±14.06</b>	<b>10.83±5.01</b>

terms of DSC, the performance gain in the tuple T1c- FLAIR is nearly 3%, whereas the improvement in the all-modalities scenario is close to 8%. If we also include the cross-modality equivariance term during training (Eq. 4) the performance is further increased, with values ranging from 3% to 4.5%.

3) *Ablation study on equivariance:* Theoretically, we can employ any spatial transformation  $\pi(\cdot)$  to explicitly enforce equivariant constraints. Nevertheless, in practice, not all the affine transformations impact each modality equally. Thus, we assess the effect of several affine transformations in this ablation study, whose results are depicted in Fig 3. We can observe several interesting observations. First, there exist transformations that always improve the performance over the baseline (e.g., rotation), whereas others either enhance or degrade the results depending on the target modality (e.g., flipping, scaling and translation). Furthermore, this negative impact is not consistent across modalities. For example, using translation as equivariance constraint degrades the performance on T1 and while has a positive effect on T2, T1c and FLAIR. On the other hand, scaling the images boosts the performance on T1, T1c and T2, but it has a degrading effect on FLAIR. Thus, finding a set of ideal affine transformations that work well across modalities is not straightforward, as demonstrated in this experiment. This motivates us to employ jointly all the transformations.

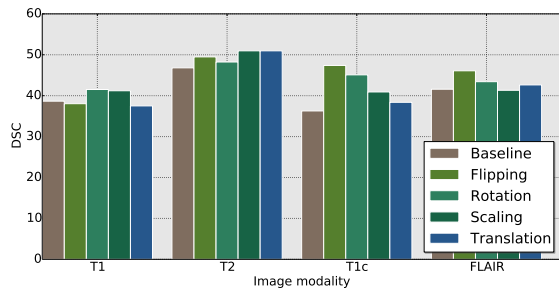


**Fig. 3:** Impact on predictions when several transformations are employed in the equivariant constraints.

4) *Robustness to backbone:* In this section we evaluate whether changes in the segmentation backbone impact the trend observed in the main results. In Table IV, it can be observed that if we replace UNet by DeepLabv3 [66] with ResNet-50 as backbone, the gap between the proposed method and prior literature still holds, being larger in some cases. For example, in the T1-T2 and T1c-FLAIR pairs, differences between our approach and SEAM [17] (all) range from 6.5% to 12% with DeepLabv3 as backbone, where the difference was of 5% and 6%, respectively, with UNet. This suggests that our learning strategy is model-agnostic and can be employed with any segmentation network.

**TABLE IV:** Results, in terms of DSC, with DeepLabv3 as backbone architecture. Best results are highlighted in bold.

Method	T1-T2	T1c-FLAIR	T1-FLAIR	T1c-T2	
CAM	Baseline	50.07±13.46	48.26±14.73	49.42±12.69	48.72±15.39
	SEAM [17] (scale)	52.01±14.21	51.43±15.27	54.27±13.58	52.60±13.23
	SEAM [17] (all)	54.38±14.04	51.09±12.18	54.21±11.49	57.65±14.73
	Proposed	<b>60.78±11.05</b>	<b>62.32±14.23</b>	<b>62.34±11.88</b>	<b>60.92±13.38</b>
GradCAM++	Baseline	49.98±13.47	48.16±14.94	49.49±12.86	48.42±15.38
	SEAM [17] (scale)	52.07±14.19	50.34±15.45	53.62±13.74	52.62±13.24
	SEAM [17] (all)	54.20±14.12	50.47±13.11	54.13±11.58	56.55±15.82
	Proposed	<b>60.95±10.97</b>	<b>62.40±14.32</b>	<b>60.08±11.85</b>	<b>60.20±14.30</b>

5) *Source of improvement:* Qualitatively (e.g., Fig 1 and 5), we can observe that the improvement on CAMs arises from better coverage of activated regions and a reduction of over-activated areas. Nevertheless, to further investigate the source of improvement, we depict in Figure 4 the variation of the DSC across different threshold values selected to binarize the obtained CAMs for each modality. First, we can observe that the proposed approach generates CAMs which bring consistent improvements across the threshold values, compared to prior works. Then, for some modalities, e.g., T1, T2 or FLAIR our approach generates CAMs whose best thresholds are centered around 0.5. This suggests that cross-modality information flow might activate under-activated regions and suppress over-activations of the single-modality baselines, resulting in more consistent CAMs across all thresholds.

To quantitatively validate this hypothesis, we compute the

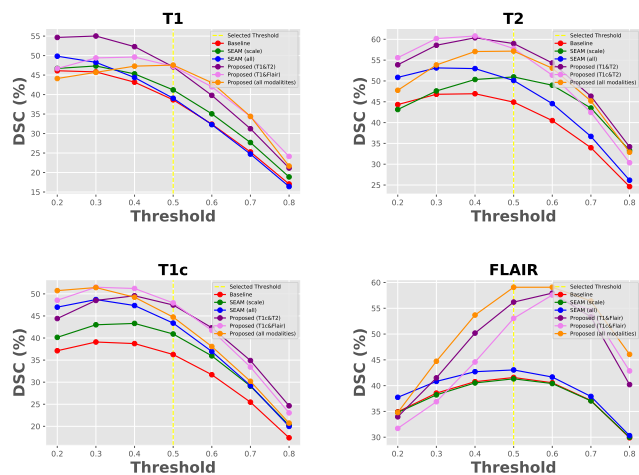


Fig. 4: Variation of DSC with respect to the threshold selected to generate the CAMs in each modality. We employ three lines to represent our methods: two for the two-modalities setting and one for the four-modality case. Note that the other approaches do not leverage multi-modal information.

TABLE V: Ratios highlighting the source of improvement. Best results in bold.

Modality	Ratio	SEAM [17](scale)	SEAM [17](all)	Proposed
T1	$r_u$	3.65	3.55	<b>2.33</b>
	$r_o$	3.51	2.49	<b>1.93</b>
T2	$r_u$	1.59	1.72	<b>0.94</b>
	$r_o$	2.07	1.38	<b>0.76</b>
T1c	$r_u$	2.64	2.58	<b>2.42</b>
	$r_o$	2.40	2.47	<b>1.89</b>
FLAIR	$r_u$	1.76	1.31	<b>0.73</b>
	$r_o$	2.17	2.54	<b>0.81</b>

ratio between False Negatives (FN) and True Positives (TP), i.e.,  $r_u = FN/TP$  and the ratio between False Positives (FP) and TP, i.e.,  $r_o = FP/TP$  with the threshold set to 0.5. Large number of FN will indicate potential under segmentations, whereas large number of FP represents over-segmented CAMs. Thus, the larger the values of these ratios the worst the generated CAMs. We report in Table V the computed  $r_u$  and  $r_o$  ratios across the different modalities compared to the SEAM method. As expected, the proposed model generates the lowest scores for both ratios, which is consistent across modalities, indicating that our approach reduces over-activated pixels while covers more complete regions. This proves that the intra and cross-modality equivariant constraints proposed in this work positively contribute during learning, leading to noticeable CAM improvements.

## B. Qualitative results

Figure 5 depicts the visual results across different models. We can observe that the original CAMs (*first column*) typically results in undersegmented regions, which aligns with the observations in the literature. Integrating single-modality equivariant constraints (i.e., SEAM [17]) has shown to improve the quantitative performance. Nevertheless, as we can observe in these images, this does not translate into a significant enhancement in terms of visual results. Indeed, SEAM based models slightly expand the initial CAMs across all the modalities, particularly in T1c and FLAIR. Nevertheless, the region

coverage by this model still misses large lesion areas. Finally, it can be observed that the CAMs generated by our model better align with the ground truth. This improvement stems not only from more complete activated regions (in all the modalities) but also from a reduction in over-activated areas (in FLAIR).

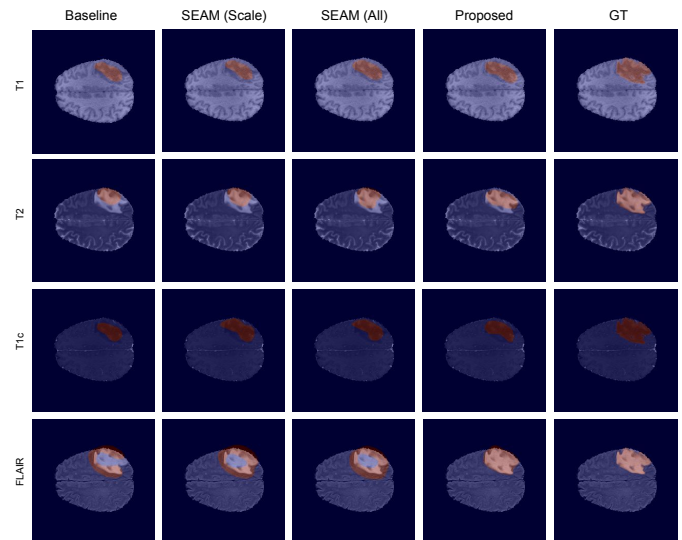


Fig. 5: Qualitative results on a given test scan (binarized CAM is overlaid on the original image). Rows represent the modality whereas the different models, as well as the corresponding ground truth are shown in columns.

## VI. CONCLUSION

We proposed a novel learning strategy for multi-modal image segmentation under the weakly supervised learning paradigm. Whereas previous methods have overlooked the use of complimentary information across modalities, here we leverage their commonalities through the integration of explicit equivariant constraints. Our experiments show that the proposed method obtains better class activation maps than prior state-of-the-art approaches. Furthermore, the source of improvement is analyzed, proving that our approach generates better CAMs by means of reducing over-activated pixels while covering more complete regions. We believe this work might raise the interest on novel learning approaches to better model intra-modality information in segmentation neural networks, particularly in the medical domain, where multi-modal imaging is a common scenario.

## ACKNOWLEDGMENTS

We would like to acknowledge Compute Canada for providing the computing resources employed in this work.

## REFERENCES

- [1] F. Milletari, N. Navab, and S.-A. Ahmadi, "V-net: Fully convolutional neural networks for volumetric medical image segmentation," in *2016 fourth international conference on 3D vision (3DV)*. IEEE, 2016, pp. 565–571. 1



- [2] J. Dolz, C. Desrosiers, and I. Ben Ayed, “3D fully convolutional networks for subcortical segmentation in MRI: A large-scale study,” *NeuroImage*, vol. 170, pp. 456–470, 2018. 1
- [3] H. Chen, Q. Dou, L. Yu, J. Qin, and P.-A. Heng, “VoxResNet: Deep voxelwise residual networks for brain segmentation from 3D MR images,” *NeuroImage*, vol. 170, pp. 446–455, 2018. 1
- [4] P. O. Pinheiro and R. Collobert, “From image-level to pixel-level labeling with convolutional networks,” in *Proceedings of the IEEE conference on computer vision and pattern recognition*, 2015, pp. 1713–1721. 1, 2
- [5] A. Bearman, O. Russakovsky, V. Ferrari, and L. Fei-Fei, “What’s the point: Semantic segmentation with point supervision,” in *European conference on computer vision*, 2016, pp. 549–565. 1
- [6] D. Lin, J. Dai, J. Jia, K. He, and J. Sun, “Scribblesup: Scribble-supervised convolutional networks for semantic segmentation,” in *Proceedings of the IEEE Conference on Computer Vision and Pattern Recognition*, 2016, pp. 3159–3167. 1, 2
- [7] M. Rajchl *et al.*, “Deepcut: Object segmentation from bounding box annotations using convolutional neural networks,” *IEEE transactions on medical imaging*, vol. 36, no. 2, pp. 674–683, 2016. 1, 2
- [8] H. Kervadec, J. Dolz, S. Wang, E. Granger, and I. ben Ayed, “Bounding boxes for weakly supervised segmentation: Global constraints get close to full supervision,” in *Medical Imaging with Deep Learning*, 2020. 1, 2
- [9] D. Pathak, P. Krahenbuhl, and T. Darrell, “Constrained convolutional neural networks for weakly supervised segmentation,” in *Proceedings of the IEEE international conference on computer vision*, 2015, pp. 1796–1804. 1, 2
- [10] H. Kervadec, J. Dolz, M. Tang, E. Granger, Y. Boykov, and I. Ben Ayed, “Constrained-CNN losses for weakly supervised segmentation,” *Medical image analysis*, vol. 54, pp. 88–99, 2019. 1, 2
- [11] H. Kervadec, J. Dolz, É. Granger, and I. Ben Ayed, “Curriculum semi-supervised segmentation,” in *International Conference on Medical Image Computing and Computer-Assisted Intervention*, 2019, pp. 568–576. 1, 2
- [12] J. Peng, H. Kervadec, J. Dolz, I. B. Ayed, M. Pedersoli, and C. Desrosiers, “Discretely-constrained deep network for weakly supervised segmentation,” *Neural Networks*, vol. 130, pp. 297–308, 2020. 1
- [13] B. Zhou, A. Khosla, A. Lapedrizza, A. Oliva, and A. Torralba, “Learning deep features for discriminative localization,” in *Proceedings of the IEEE conference on computer vision and pattern recognition*, 2016, pp. 2921–2929. 1, 3, 5
- [14] S. J. Oh, R. Benenson, A. Khoreva, Z. Akata, M. Fritz, and B. Schiele, “Exploiting saliency for object segmentation from image level labels,” in *2017 IEEE conference on computer vision and pattern recognition (CVPR)*. IEEE, 2017, pp. 5038–5047. 1, 2
- [15] J. Fan, Z. Zhang, C. Song, and T. Tan, “Learning integral objects with intra-class discriminator for weakly-supervised semantic segmentation,” in *Proceedings of the IEEE Conference on Computer Vision and Pattern Recognition*, 2020, pp. 4283–4292. 1, 2
- [16] Y. Wei, J. Feng, X. Liang, M.-M. Cheng, Y. Zhao, and S. Yan, “Object region mining with adversarial erasing: A simple classification to semantic segmentation approach,” in *Proceedings of the IEEE conference on computer vision and pattern recognition*, 2017, pp. 1568–1576. 1, 2
- [17] Y. Wang, J. Zhang, M. Kan, S. Shan, and X. Chen, “Self-supervised equivariant attention mechanism for weakly supervised semantic segmentation,” in *Proceedings of the IEEE Conference on Computer Vision and Pattern Recognition*, 2020, pp. 12 275–12 284. 1, 2, 4, 5, 6, 7, 8
- [18] A. Kolesnikov and C. H. Lampert, “Seed, expand and constrain: Three principles for weakly-supervised image segmentation,” in *European conference on computer vision*. Springer, 2016, pp. 695–711. 2
- [19] J. Dai, K. He, and J. Sun, “Boxsup: Exploiting bounding boxes to supervise convolutional networks for semantic segmentation,” in *Proceedings of the IEEE international conference on computer vision*, 2015, pp. 1635–1643. 2
- [20] A. Khoreva, R. Benenson, J. Hosang, M. Hein, and B. Schiele, “Simple does it: Weakly supervised instance and semantic segmentation,” in *Proceedings of the IEEE conference on computer vision and pattern recognition*, 2017, pp. 876–885. 2
- [21] Y. Zhang, P. David, and B. Gong, “Curriculum domain adaptation for semantic segmentation of urban scenes,” in *Proceedings of the IEEE International Conference on Computer Vision*, 2017, pp. 2020–2030. 2
- [22] T. Remez, J. Huang, and M. Brown, “Learning to segment via cut-and-paste,” in *Proceedings of the European conference on computer vision (ECCV)*, 2018, pp. 37–52. 2
- [23] Q. Hou, M.-M. Cheng, X. Hu, A. Borji, Z. Tu, and P. H. Torr, “Deeply supervised salient object detection with short connections,” in *Proceedings of the IEEE conference on computer vision and pattern recognition*, 2017, pp. 3203–3212. 2
- [24] G. Li, Y. Xie, L. Lin, and Y. Yu, “Instance-level salient object segmentation,” in *Proceedings of the IEEE Conference on Computer Vision and Pattern Recognition*, 2017, pp. 2386–2395. 2
- [25] M. Tang, F. Perazzi, A. Djelouah, I. Ben Ayed, C. Schroers, and Y. Boykov, “On regularized losses for weakly-supervised cnn segmentation,” in *Proceedings of the European Conference on Computer Vision (ECCV)*, 2018, pp. 507–522. 2
- [26] R. R. Selvaraju, M. Cogswell, A. Das, R. Vedantam, D. Parikh, and D. Batra, “Grad-cam: Visual explanations from deep networks via gradient-based localization,” in *Proceedings of the IEEE international conference on computer vision*, 2017, pp. 618–626. 2
- [27] K. Simonyan, A. Vedaldi, and A. Zisserman, “Deep inside convolutional networks: Visualising image classification models and saliency maps,” *arXiv preprint arXiv:1312.6034*, 2013. 2
- [28] X. Wang, S. You, X. Li, and H. Ma, “Weakly-supervised semantic segmentation by iteratively mining common object features,” in *Proceedings of the IEEE Conference on Computer Vision and Pattern Recognition*, 2018, pp. 1354–1362. 2
- [29] G. Papandreou, L.-C. Chen, K. P. Murphy, and A. L. Yuille, “Weakly- and semi-supervised learning of a deep convolutional network for semantic image segmentation,” in *Proceedings of the IEEE international conference on computer vision*, 2015, pp. 1742–1750. 2
- [30] C. Rother, V. Kolmogorov, and A. Blake, ““ grabcut” interactive foreground extraction using iterated graph cuts,” *ACM transactions on graphics (TOG)*, vol. 23, no. 3, pp. 309–314, 2004. 2
- [31] K. Wu, B. Du, M. Luo, H. Wen, Y. Shen, and J. Feng, “Weakly supervised brain lesion segmentation via attentional representation learning,” in *International Conference on Medical Image Computing and Computer-Assisted Intervention*, 2019, pp. 211–219. 2
- [32] H.-G. Nguyen *et al.*, “A novel segmentation framework for uveal melanoma in magnetic resonance imaging based on class activation maps,” in *International Conference on Medical Imaging with Deep Learning*. PMLR, 2019, pp. 370–379. 2
- [33] X. Ouyang *et al.*, “Weakly supervised segmentation framework with uncertainty: A study on pneumothorax segmentation in chest x-ray,” in *International Conference on Medical Image Computing and Computer-Assisted Intervention*, 2019, pp. 613–621. 2
- [34] Z. Jia, X. Huang, E. I. Chang, and Y. Xu, “Constrained deep weak supervision for histopathology image segmentation,” *IEEE Transactions on Medical Imaging*, vol. 36, no. 11, pp. 2376–2388, 2017. 2
- [35] S. Gidaris, P. Singh, and N. Komodakis, “Unsupervised representation learning by predicting image rotations,” in *ICLR*, 2018. 2
- [36] C. Doersch, A. Gupta, and A. A. Efros, “Unsupervised visual representation learning by context prediction,” in *Proceedings of the IEEE international conference on computer vision*, 2015, pp. 1422–1430. 2
- [37] M. Noroozi and P. Favaro, “Unsupervised learning of visual representations by solving jigsaw puzzles,” in *European conference on computer vision*, 2016, pp. 69–84. 2
- [38] D. Pathak, P. Krahenbuhl, J. Donahue, T. Darrell, and A. A. Efros, “Context encoders: Feature learning by inpainting,” in *Proceedings of the IEEE conference on computer vision and pattern recognition*, 2016, pp. 2536–2544. 2
- [39] G. Larsson, M. Maire, and G. Shakhnarovich, “Learning representations for automatic colorization,” in *European conference on computer vision*, 2016, pp. 577–593. 2
- [40] A. Dosovitskiy, J. T. Springenberg, M. Riedmiller, and T. Brox, “Discriminative unsupervised feature learning with convolutional neural networks,” 2014. 2
- [41] C. Doersch and A. Zisserman, “Multi-task self-supervised visual learning,” in *Proceedings of the IEEE International Conference on Computer Vision*, 2017, pp. 2051–2060. 2
- [42] R. Zhang, P. Isola, and A. A. Efros, “Split-brain autoencoders: Unsupervised learning by cross-channel prediction,” in *Proceedings of the IEEE Conference on Computer Vision and Pattern Recognition*, 2017, pp. 1058–1067. 2
- [43] K. Chaitanya, E. Erdil, N. Karani, and E. Konukoglu, “Contrastive learning of global and local features for medical image segmentation with limited annotations,” in *NeurIPS*, 2020. 2
- [44] J. Thewlis, H. Bilen, and A. Vedaldi, “Unsupervised learning of object landmarks by factorized spatial embeddings,” in *Proceedings of the IEEE international conference on computer vision*, 2017, pp. 5916–5925. 2
- [45] Y. Wang, J. Zhang, M. Kan, S. Shan, and X. Chen, “Self-supervised scale equivariant network for weakly supervised semantic segmentation,” *arXiv preprint arXiv:1909.03714*, 2019. 2

- [46] M. Sahasrabudhe *et al.*, “Self-supervised nuclei segmentation in histopathological images using attention,” in *International Conference on Medical Image Computing and Computer-Assisted Intervention*, 2020, pp. 393–402. 2, 4
- [47] W.-C. Hung, V. Jampani, S. Liu, P. Molchanov, M.-H. Yang, and J. Kautz, “Scops: Self-supervised co-part segmentation,” in *Proceedings of the IEEE Conference on Computer Vision and Pattern Recognition*, 2019, pp. 869–878. 2
- [48] X. Li, L. Yu, H. Chen, C.-W. Fu, L. Xing, and P.-A. Heng, “Transformation-consistent self-ensembling model for semisupervised medical image segmentation,” *IEEE Transactions on Neural Networks and Learning Systems*, 2020. 2
- [49] P. Moeskops, M. A. Viergever, A. M. Mendrik, L. S. De Vries, M. J. Benders, and I. Išgum, “Automatic segmentation of mr brain images with a convolutional neural network,” *IEEE transactions on medical imaging*, vol. 35, no. 5, pp. 1252–1261, 2016. 3
- [50] W. Zhang *et al.*, “Deep convolutional neural networks for multi-modality isointense infant brain image segmentation,” *NeuroImage*, vol. 108, pp. 214–224, 2015. 3
- [51] D. Nie, L. Wang, Y. Gao, and D. Shen, “Fully convolutional networks for multi-modality isointense infant brain image segmentation,” in *2016 IEEE 13th international symposium on biomedical imaging (ISBI)*. IEEE, 2016, pp. 1342–1345. 3
- [52] X. Li *et al.*, “3D multi-scale FCN with random modality voxel dropout learning for intervertebral disc localization and segmentation from multi-modality mr images,” *Medical image analysis*, vol. 45, pp. 41–54, 2018. 3
- [53] J. Dolz, K. Gopinath, J. Yuan, H. Lombaert, C. Desrosiers, and I. B. Ayed, “Hyperdense-Net: a hyper-densely connected CNN for multi-modal image segmentation,” *IEEE transactions on medical imaging*, vol. 38, no. 5, pp. 1116–1126, 2018. 3
- [54] J. Li, Z. L. Yu, Z. Gu, H. Liu, and Y. Li, “MMAN: Multi-modality aggregation network for brain segmentation from MR images,” *Neuro-computing*, vol. 358, pp. 10–19, 2019. 3
- [55] X. Zhang, Y. Wei, J. Feng, Y. Yang, and T. S. Huang, “Adversarial complementary learning for weakly supervised object localization,” in *Proceedings of the IEEE Conference on Computer Vision and Pattern Recognition*, 2018, pp. 1325–1334. 3
- [56] S. Gupta, J. Hoffman, and J. Malik, “Cross modal distillation for supervision transfer,” in *Proceedings of the IEEE conference on computer vision and pattern recognition*, 2016, pp. 2827–2836. 4
- [57] Y. Zhang, T. Xiang, T. M. Hospedales, and H. Lu, “Deep mutual learning,” in *Proceedings of the IEEE Conference on Computer Vision and Pattern Recognition*, 2018, pp. 4320–4328. 4
- [58] S. Zagoruyko and N. Komodakis, “Paying more attention to attention: Improving the performance of convolutional neural networks via attention transfer,” in *ICLR*, 2017. 4
- [59] S. Bakas *et al.*, “Advancing the cancer genome atlas glioma mri collections with expert segmentation labels and radiomic features,” *Scientific data*, vol. 4, p. 170117, 2017. 5
- [60] R. Bakas *et al.*, “Identifying the best machine learning algorithms for brain tumor segmentation, progression assessment, and overall survival prediction in the brats challenge,” *arXiv:1811.02629*, 2018. 5
- [61] B. H. Menze *et al.*, “The multimodal brain tumor image segmentation benchmark (brats),” *IEEE transactions on medical imaging*, vol. 34, no. 10, pp. 1993–2024, 2014. 5
- [62] A. Paszke *et al.*, “Pytorch: An imperative style, high-performance deep learning library,” in *NeurIPS*, 2019. 5
- [63] O. Ronneberger, P. Fischer, and T. Brox, “U-net: Convolutional networks for biomedical image segmentation,” in *International Conference on Medical image computing and computer-assisted intervention*, 2015, pp. 234–241. 5
- [64] I. Loshchilov and F. Hutter, “Decoupled weight decay regularization,” in *International Conference on Learning Representations*, 2019. 5
- [65] A. Chattopadhyay, A. Sarkar, P. Howlader, and V. N. Balasubramanian, “Grad-cam++: Generalized gradient-based visual explanations for deep convolutional networks,” in *2018 IEEE Winter Conference on Applications of Computer Vision (WACV)*, 2018, pp. 839–847. 5
- [66] L.-C. Chen, G. Papandreou, F. Schroff, and H. Adam, “Rethinking atrous convolution for semantic image segmentation,” *arXiv preprint arXiv:1706.05587*, 2017. 7